ACS OMEGA

http://pubs.acs.org/journal/acsodf

Article

High-Yield Gold Nanohydrangeas on Three-Dimensional Carbon Nanotube Foams for Surface-Enhanced Raman Scattering Sensors

Rong Yang, Zhen Zhang, Naiqian Miao, Weichen Fang, Zuo Xiao, Xiaodong Shen, and Wenbo Xin*

Cite This: *ACS Omega* 2023, 8, 26973−26981

Read Online

ACCESS | Metrics & More | Article Recommendations | Supporting Information

ABSTRACT: Recently, carbon nanomaterial-supported plasmonic nanocrystals used as high-performance surface-enhanced Raman scattering (SERS) substrates have attracted increasing attention due to their ultra-high sensitivity of detection. However, most of the work focuses on the design of 2-D planar substrates with traditional plasmonic structures, such as nanoparticles, nanorods, nanowires, and so forth. Here, we report a novel strategy for the preparation of high-yield Au nanohydrangeas on three-dimensional porous polydopamine (PDA)/polyvinyl alcohol (PVA)/carbon nanotube (CNT) foams. The structures and growth mechanisms of these specific Au nanocrystals are systematically investigated. PDA plays the role of both a reducing agent as well as an anchoring site for Au nanohydrangeas' growth. We also show that the ratio of surfactant KBr to the gold precursor ($HAuCl_4$) is key to obtain these structures in a manner of high production. Moreover, the substrate of the CNT foam−Au nanohydrangea hybrid can be employed as SERS sensors and can detect the analytes down to 10^{-9} M.

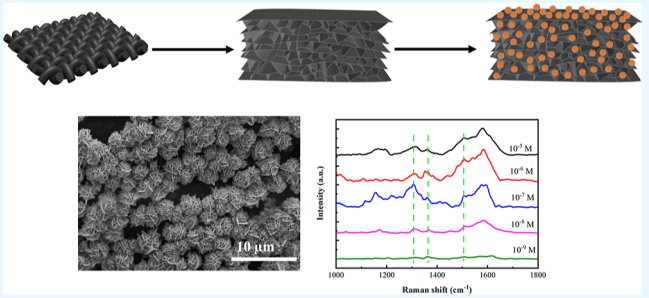

INTRODUCTION

Surface-enhanced Raman scattering (SERS) is a powerful detection technique that is more sensitive than Raman spectroscopy and facilitates the detection of ultralow concentrations or even single-molecule analytes,[1] which is widely used in food safety,[2,3] environmental monitoring,[4,5] and trace analysis.[6,7] The Raman signal of the analytes is greatly amplified on the SERS substrate owing to the enhancement effect of the electromagnetic field when the electromagnetic wave is excited on the plasmonic surface,[8] that is, the electromagnetic enhancement mechanism (EM). The chemical enhancement mechanism works when the adsorbed molecule undergoes electron transfer with the plasmonic noble metal substrates. However, it is now generally believed that most SERS signal enhancement process is mainly from the EM.[9] The intensity of the electromagnetic field is related to the shape, size, sharp edges, tips, and the gap between the plasmonic nanostructures, named "hotspots".[10] A wide range of studies have been conducted on the structural control of noble metal nanocrystals to achieve ultra-sensitive SERS performance. For instance, gold (Au) nanoparticles,[11] nanoplates,[12] nanobelts,[13,14] dendrites,[15] and so forth. have been precisely synthesized and employed as high-performance SERS substrates. Among these structures, 3-D structures like stars,[16−19] dendrites,[20,21] and flowers,[22−24] show outstanding performance when used as SERS substrates because they possess high-density hotspots, which can generate a strong enough intensity of the electromagnetic field.[25] Therefore, compared to nanoparticles, the controllable synthesis of high-yield 3-D plasmonic structures is of significance for robust SERS applications.

Nanoflowers have a representative structure of these 3-D plasmonic nanocrystals, presenting ultra-sensitive SERS signals.[26,27] For the construction of flower-like structures, many synthesis methods have been reported. For example, Guo et al. proposed a rapid synthesis route to deposit Au nanoflowers on the surface of tin-doped indium oxide glass by the electrochemical deposition method.[28] Wu et al. grew silver nanoflowers directly on the patterned wafers prepared by the optical interference method.[29] On the other hand, Pradhan et al. prepared Au nanoflowers using galvanic replacement between polystyrene bead-supported Cu nanoparticles and $HAuCl_4$.[30] However, most of these flower-like structures are decorated on 2-D support materials like rigid glasses[28] or flexible polymer films,[31] which are nearly planar and have limited surface areas to accommodate sufficient plasmonic structures and to create high-density hotspots. From this point of view, 3-D porous materials like aerogels possess a super-large specific surface area, high porosity, and ultralow

Received: March 16, 2023
Accepted: July 7, 2023
Published: July 21, 2023

density,[32−34] which is a promising candidate for building SERS substrates.

Hence, we propose a novel synthesis route for the growth of 3-D hydrangea-like Au nanoflowers on porous polydopamine (PDA)/poly(vinyl alcohol) (PVA)/carbon nanotube (CNT) foams. We first fabricate a CNT foam with a high specific surface area and numerous micropores, providing sufficient space for the growth of Au nanocrystals. Meanwhile, we functionalize the CNT foam with a combo recipe of PVA and PDA. The polymer coating process makes the foam surface full of catechol and amino groups, which can not only promote the in situ reduction of Au ions but also realize the strong adsorption of Au atoms.[35] In addition, the potassium bromide (KBr) serving as the surfactant directs the anisotropic growth of Au nanoparticles to obtain the hydrangea-like structure. We further investigate the growth mechanism of these interesting Au structures by modifying the synthesis conditions. Finally, we devise a SERS substrate based on the CNT foam−Au nanohydrangea hybrid platform, which provides detection sensitivity of the analyte rhodamine 6G (R6G) down to 10^{-9} M.

EXPERIMENTAL SECTION

Chemicals and Materials. CNT sheets were purchased from Suzhou Jernano Carbon Co., Ltd., China. Hydrochloric acid (HCl, 38%) and hydrogen peroxide (H_2O_2, ≥30%) were purchased from Shanghai Lingfeng Chemical Reagent Co., Ltd., China. Sodium hydroxide (NaOH, AR) was purchased from Sinopharm Chemical Reagent Co., Ltd., China. Polyvinyl alcohol (PVA, alcoholysis degree 97.5−99%), dimethyl sulfoxide (DMSO, 99%), dopamine hydrochloride (DA), tris-hydrochloride buffer (Tris-HCl, 1 M, pH = 8.5), and gold chloride trihydrate ($HAuCl_4{\cdot}3H_2O$, ≥99.9%) were purchased from Shanghai Aladdin Biochemical Technology Co., Ltd., China. Potassium bromide (KBr) was purchased from Sigma-Aldrich, USA. Rhodamine 6G (R6G, 99%) was purchased from Thermo Fisher Scientific, China.

Preparation of the PDA/PVA/CNT Foam. In brief, three-dimensional CNT foam was fabricated by exfoliating a two-dimensional CNT film in an oxidation solution (containing H_2O_2 and HCl), followed by neutralization with a NaOH solution. After that, the wet CNT foam was soaked in PVA solution (20 mg/mL dissolved in 90% DMSO solution) and stirred for 30 min at room temperature, followed by the freeze-drying process. Then, the PVA/CNT foam was heated at 180 °C for 1 h to avoid the PVA coating from dissolving again as PVA is a kind of water-soluble polymer. Finally, the PDA/PVA/CNT foam was prepared by soaking the PVA/CNT foam in DA solutions with different concentrations (0, 2, 5, and 10 mg/mL dissolved in a 10 mM Tris-HCl solution with pH = 8.5) and stirring for 15 h at room temperature and then washed with deionized water. After the freeze-drying process, the PDA/PVA/CNT foam was formed.

Preparation of Au Nanohydrangeas on the PDA/PVA/CNT Foam. Typically, 47.5 mL of deionized water was transferred to a glass beaker. Then, 1.25 mL of $HAuCl_4$ (100 mM) and 1.25 mL of KBr (50 mM) were added to the beaker. When the solution was evenly mixed, the PDA/PVA/CNT foam was soaked in it for 4 h. Afterward, the PDA/PVA/CNT foam was taken out and washed with deionized water. Finally, the PDA/PVA/CNT foam−Au nanohydrangea hybrid was obtained by the freeze-drying process. Without a special note, Au nanohydrangeas were synthesized on PDA/PVA/CNT foams treated with DA at 5 mg/mL. To investigate the function of PDA coating in Au nanohydrangea growth, the PDA/PVA/CNT foams prepared by 0, 2, 5, and 10 mg/mL DA were immersed in the Au precursor solution under the same conditions as those in the preparation of the PDA/PVA/CNT foam−Au nanohydrangea hybrid. In addition to PDA coating, the concentration of $HAuCl_4$ also affects the morphology of Au nanohydrangeas. So, we fabricated the extra solutions with 0.75, 2.5, and 5 mL of $HAuCl_4$ (100 mM) under the same conditions as those in the preparation of the PDA/PVA/CNT foam−Au nanohydrangea hybrid. To study the role of KBr on the growth of Au nanohydrangeas, the extra solutions with 0, 0.5, and 5 mL of KBr (50 mM) were fabricated following the typical process with the same parameters.

Characterizations. Scanning electron microscopy (SEM) images were obtained using Zeiss Supra 55, Zeiss Sigma 500, and SNE-4500M. Elemental mapping of the PDA/PVA/CNT foam−Au nanohydrangeas was performed on SEM coupled with energy-dispersive X-ray spectroscopy (SEM/EDS), which was obtained using Zeiss Supra 55. Transmission electron microscopy (TEM) and high-resolution TEM (HRTEM) images were obtained using JEM 2100F. X-ray diffraction (XRD) analysis was performed on a Bruker D2 Phaser diffractometer using Cu Kα1 radiation.

SERS Performance. To study the SERS performance of the PDA/PVA/CNT foam−Au nanohydrangea hybrid, we employed the R6G as the analytes to immerse the substrate into the R6G solution with the concentrations ranging from 1×10^{-5} to 1×10^{-10} M for 0.5 h. After drying, the substrate was transferred to Raman equipment for analysis. Raman spectroscopy analysis was performed on RTS2-785-N with a laser length of 785 nm and an exposure time of 10 s.

RESULTS AND DISCUSSION

To obtain the 3-D porous structure of the CNT foam, we employ a 2-D CNT film as the start material, as shown in Figure S1a. The morphology analysis shows a well-organized 2-D surface of CNT assembly made of numerous CNTs and CNT bundles. Occasionally, a few wrinkles and impurities can be noted on the surface of the CNT film. The CNT foam is spontaneously fabricated by exfoliating the CNT film in a mixed oxidation solution of HCl and H_2O_2. The well-established 3-D CNT porous structure is further treated with PVA and PDA sequentially in the solution to obtain the PDA/PVA/CNT foam hybrid. More experimental details can be found in the Experimental Section. We note that the PVA coating can not only provide the mechanical properties for the CNT foam but also modify CNT surfaces to better accommodate the following PDA depositions. Meanwhile, in our process, PDA functions as the reducing agent to the Au precursor and is of importance to improve the adsorption ability of Au nanoparticles.[36,37] Figure S1b shows the SEM image of the as-fabricated 3-D PDA/PVA/CNT foam, which possesses a super-high specific surface area, porous and multilayered structure, and the pores of the foam are as big as a millimeter level. Benefiting from this unique characteristic, the composited CNT foam can provide sufficient growth space for the high-yielding growth of Au nanohydrangeas.

The synthesis of Au nanohydrangeas is based on the spontaneous redox reaction between Au ions and the PDA. During the reaction process, KBr plays the role of a surfactant to facilitate the anisotropic growth of Au nanoparticles. Figure

https://doi.org/10.1021/acsomega.3c01802
ACS Omega 2023, 8, 26973−26981

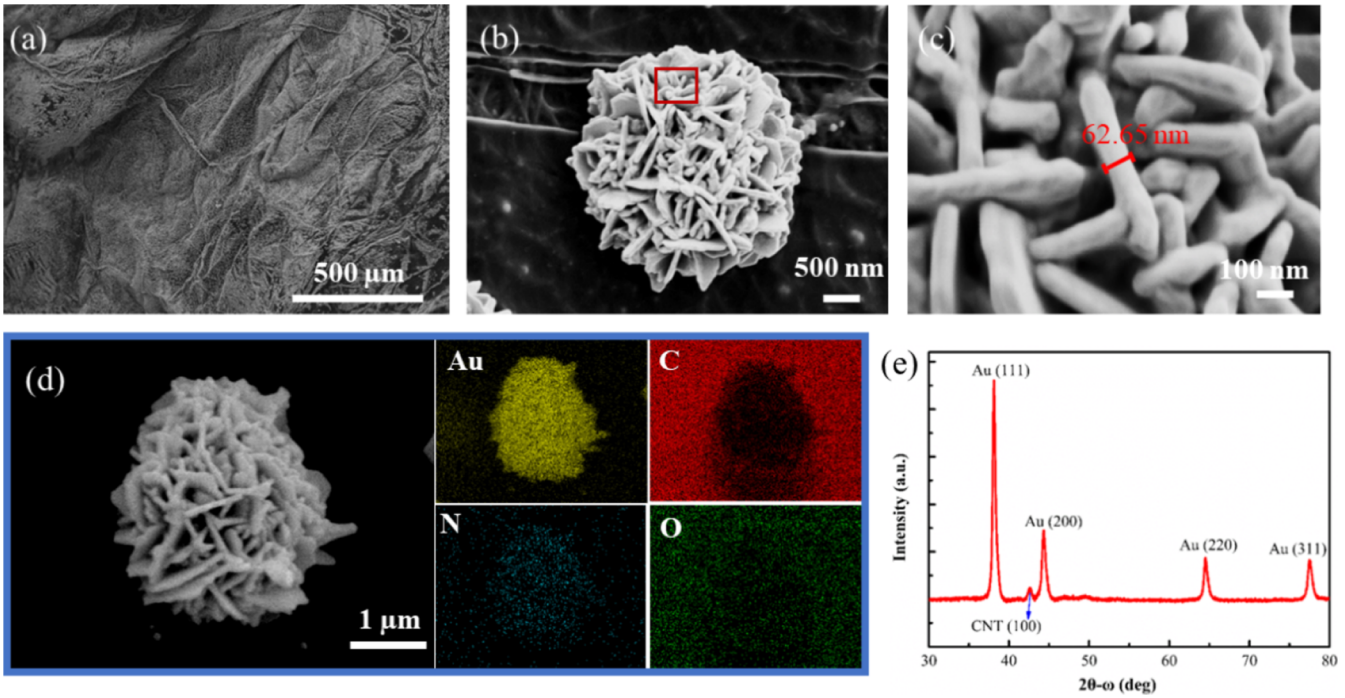

Figure 1. Structure investigation of CNT foam−Au nanohydrangeas. Representative low- (a) and high-magnification (b) SEM images of the PDA/PVA/CNT foam−Au nanohydrangea hybrid. (c) Enlarged SEM image of a selected region in (b). (d) Elemental mapping of the PDA/PVA/CNT foam−Au nanohydrangea hybrid. (e) XRD pattern of the PDA/PVA/CNT foam−Au nanohydrangea hybrid.

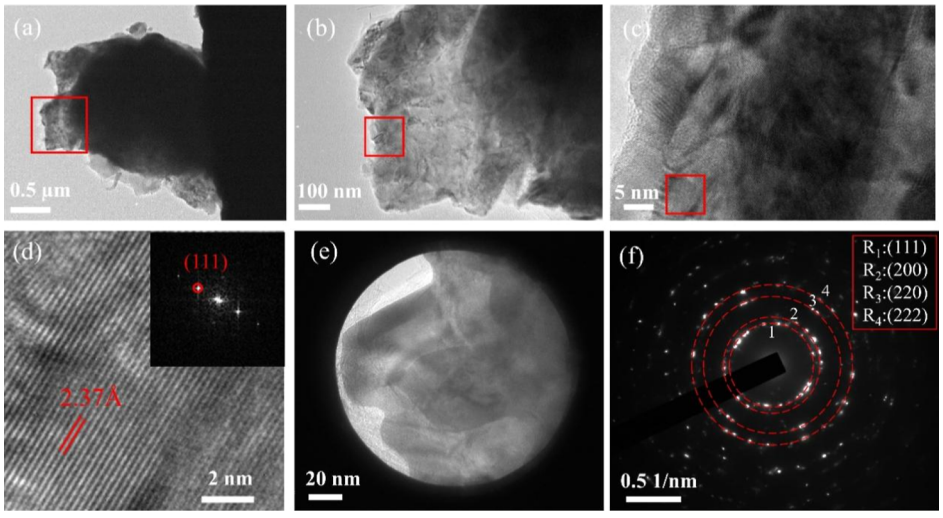

Figure 2. TEM investigation of Au nanohydrangeas. (a) Representative TEM image of a selected Au nanohydrangea on the PDA/PVA/CNT foam; (b) an enlarged image of a selected region in (a). (c) High-magnification image of a selected region in (b). (d) HRTEM image of a selected region in (c). Inset is its corresponding FFT. (e) Representative TEM image of a root of Au nanohydrangea on the PDA/PVA/CNT foam. (f) Corresponding SAED pattern of (e).

1a shows the low magnification SEM image of the Au nanohydrangeas deposited on PDA/PVA/CNT foam. It is of interest to note that we obtain high-yield Au nanohydrangeas via our synthesis route, which are homogeneously distributed on the surface of PDA/PVA/CNT foam. More interestingly, not only the surface but also the inside of the foam porosity is densely loaded with Au nanohydrangeas, as shown in Figure S2, the cross-sectional SEM image of the sample. Figure 1b exhibits the morphology of the synthesized Au nanocrystals, which are spherical in outline with a rough surface and a petal-like layered structure, resembling hydrangeas. It is worth noting that Au nanohydrangeas are composed of randomly arranged plate-like structures with a thickness of 62.65 nm, as shown in Figure 1c. EDS is employed to analyze the composition of Au nanohydrangeas. Figure 1d shows the results of elemental mapping of an integrated structure of the hydrangea. Four elements are captured, including Au (gold), C (carbon), N (nitrogen), and O (oxygen), which come from the nanohydrangea, CNT substrate, PDA coating, and possibly both CNT and polymer coating, respectively. Moreover, the elemental mapping of Au matches the spherical structure of the hydrangea in the selected region.

XRD is carried out to study the crystalline structure of Au nanohydrangeas. In Figure 1e, the XRD pattern of the PDA/

https://doi.org/10.1021/acsomega.3c01802
ACS Omega 2023, 8, 26973−26981

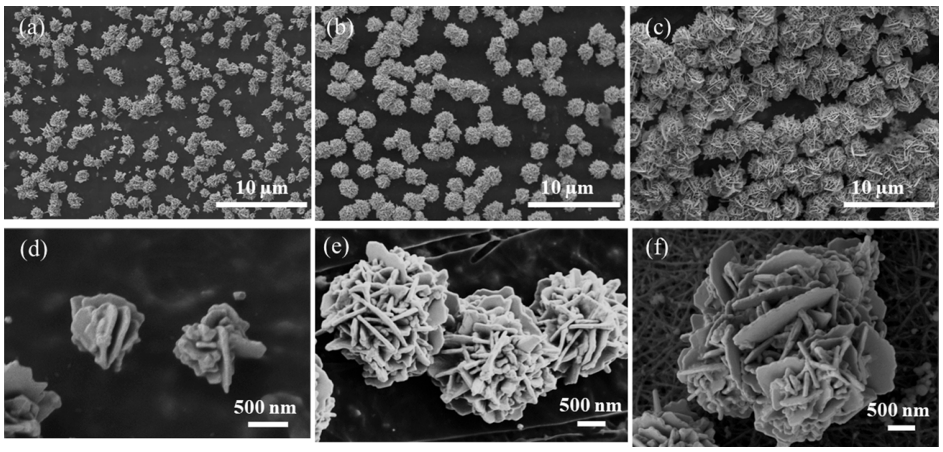

Figure 3. Representative SEM images of Au nanohydrangeas synthesized on the PDA/PVA/CNT foam with a variety of Au precursor concentrations. Low magnification: (a) 0.75, (b) 1.25, and (c) 2.5 mL of $HAuCl_4$ and high magnification: (d) 0.75, (e) 1.25, and (f) 2.5 mL of $HAuCl_4$ used in the synthesis.

PVA/CNT foam−Au nanohydrangeas hybrid shows that diffraction peaks at 38.1, 44.4, 64.5, and 77.6° correspond to the (111), (200), (220), and (311) of Au planes, respectively, which demonstrates that the fabricated nanohydrangeas are face-centered cubic (FCC) Au structures.[12,38] The diffraction peak at 42.6° corresponds to the (100) plane of the CNT.[39,40] Interestingly, the ratio of diffraction peak intensities between (200) and (111) is 0.3, lower than 0.5, which is the standard number of powdered Au polycrystalline nanocrystals. This indicates the deposited Au nanohydrangeas are (111)-oriented to some extent.[12,41]

In order to fully understand the crystalline structure of Au nanohydrangeas, TEM and HRTEM are further employed. Figure 2a exhibits the representative TEM image of a single Au nanohydrangea. The main body of the hydrangea is indeed nearly spherical, and there are many petal-like plates extending out of the outline. Figure 2b shows the HRTEM image of the petal originating from the main body, which has a relatively flat surface and uniform texture. The lattice spacing of the selected region in Figure 2c is measured, and the results are shown in Figure 2d. The lattice spacing of 2.37 Å corresponds to the (111) plane spacing of Au, which is consistent with the fast Fourier transform (FFT) results inserted in Figure 2d. It can be inferred that the petal of Au nanohydrangea is (111)-oriented single crystalline structure. In order to investigate the crystalline structure of Au nanohydrangeas more comprehensively, we also take a selected area of the root of Au nanohydrangeas (Figure 2e) and perform its electron diffraction. The typical polycrystalline diffraction rings are observed as shown in Figure 2f, which are indexed as the Bragg reflections of Au(111), (200), (220), and (222) planes, revealing that the roots of Au nanohydrangeas are polycrystalline with the FCC structure, consistent with the XRD results. Therefore, the petals of the Au nanohydrangea are (111)-oriented single-crystal structures, while its root is polycrystalline.

Our experiment identifies that PDA is one of the key factors to obtain Au nanohydrangeas. Compared to the commonly used hydrogen electrodes, the redox potential of the catechol groups in the PDA coating can reach −530 mV, which is sufficient for the reduction of Au ions.[42] To elaborate on the role of PDA, we also use only PVA-decorated CNT foam as the substrate to direct the growth of Au nanocrystals. However, we fail to find any Au nanocrystals on its surface (Figure S3). The result confirms the sufficient reducing capability of PDA in our synthesis. We further investigate the effect of PDA concentration on the morphology of Au nanohydrangeas. When the concentration of DA is as low as 2 mg/mL, the PDA content on CNT foams is so low that only a small amount of Au ions are reduced to grow into Au nanohydrangeas with low yields (Figure S4a). However, when we treat PVA/CNT foams with 5 mg/mL DA to deposit Au nanocrystals, the PDA content on the CNT foam is enough to reduce sufficient Au ions for the growth of Au nanohydrangeas. Therefore, the Au nanohydrangeas prepared under this condition have a more perfect structure and improved yields (Figure 3b). When the concentration of DA increases to 10 mg/mL, the reduction rate of Au ions is accelerated, which is not conducive to the growth of Au nanohydrangeas, resulting in more plate structures stretching out (Figure S4b). On the other hand, PDA coating maintains rich amino groups, which can provide abundant nucleation sites for the growth of Au nanocrystals because amino groups have a lone electron pair to bind metal ions through the shared electron pairs.[43] Therefore, PDA deposited on PVA/CNT foam secures the successful synthesis of high-yield Au nanohydrangeas here.

To investigate the effect of the Au precursor concentration on the morphology of Au nanohydrangeas, we perform a series of experiments by changing the concentration of $HAuCl_4$. Figure 3 shows the SEM images of the as-prepared products fabricated with 0.75, 1.25, and 2.5 mL of $HAuCl_4$ (100 mM). When the concentration of Au precursors is as low as 0.75 mL, the reduced Au atoms are insufficient to reach the saturation concentration to form well-shaped nanohydrangeas. As a result, only a few Au nanoparticles grow into small-sized Au nanohydrangeas, and most of them finally form nanoparticles with an irregular flower-like structure, just like the prototype of nanohydrangeas (Figure 3a,d). On the other hand, when the concentration of $HAuCl_4$ increases to 1.25 mL, sufficient Au ions in the system are reduced, providing enough Au atoms to nucleate and grow into Au nanohydrangeas, as shown in Figure 3b. The shape of the Au nanocrystals is well established, forming more regular hydrangea structures as shown in Figure 3e.

As expected, the loading of Au nanohydrangeas on the composite CNT foam is significantly higher when the

https://doi.org/10.1021/acsomega.3c01802
ACS Omega 2023, 8, 26973−26981

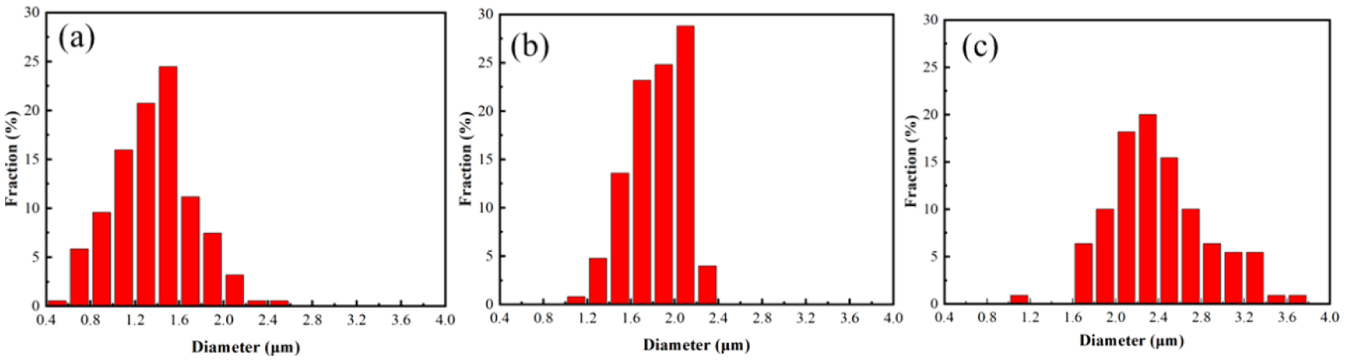

Figure 4. Size distribution of Au nanohydrangeas fabricated on the PDA/PVA/CNT foam with a variety of $HAuCl_4$ concentrations. (a) 0.75, (b) 1.25, and (c) 2.5 mL of $HAuCl_4$.

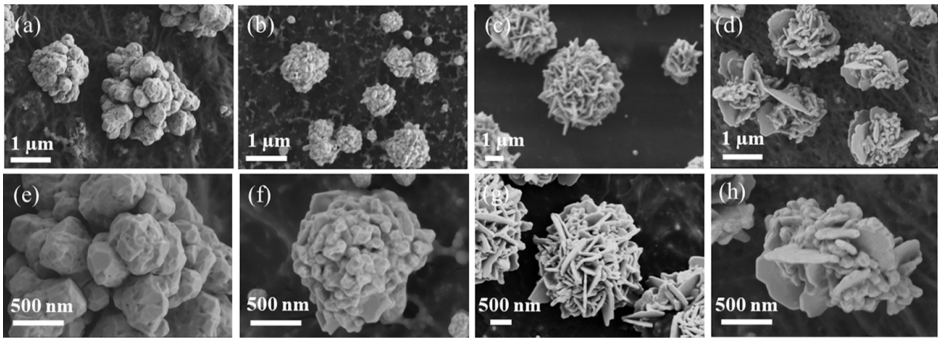

Figure 5. Representative SEM images of Au nanohydrangeas synthesized on the PDA/PVA/CNT foam with a variety of KBr concentrations. Low magnification: (a) 0, (b) 0.5, and (c) 1.25, and (d) 5 mL of KBr and high magnification: (e) 0, (f) 0.5, (g) 1.25, and (h) 5 mL of KBr.

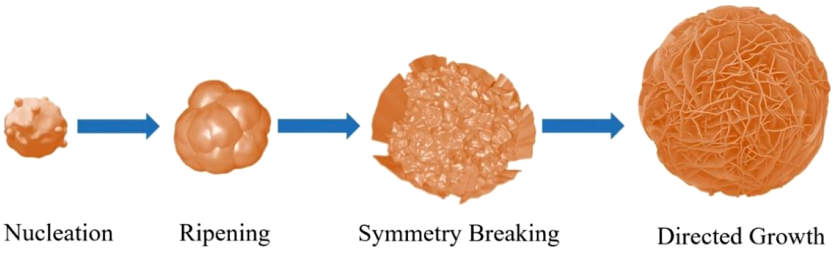

Figure 6. Schematic illustration of the growth mechanism of Au nanohydrangeas on PDA/PVA/CNT foam.

concentration of precursors is as high as 2.5 mL, and the size of individual nanohydrangeas is also remarkably larger (Figure 3c,f). Here, we calculated the yield of Au nanohydrangeas as the area occupied by Au nanohydrangeas divided by the total area of gold nanocrystals on the PDA/PVA/CNT foam in the SEM image. The result shows that the yield of Au nanohydrangeas is over 95%, and as shown in the SEM image in Figure 3c, almost no other byproducts appeared except for Au nanohydrangeas. Figure 4 shows the size distribution of Au nanohydrangeas obtained with different $HAuCl_4$ concentrations. We note that the average diameters of the synthesized Au nanocrystals are 1.36 ± 0.03, 1.87 ± 0.04, and 2.30 ± 0.03 μm with the concentration of the Au precursor at 0.75, 1.25, and 2.5 mL, respectively. The result demonstrates that the size of Au nanohydrangeas becomes larger as the concentration of $HAuCl_4$ increases. Therefore, the concentration of the Au precursor determines the size, yield, and structural integrity of Au nanohydrangeas. However, overloaded Au precursors are detrimental to the formation of hydrangea-like structures. As shown in Figure S5, when the $HAuCl_4$ loading reaches 5 mL, the yield of nanocrystals decreases dramatically with their shapes more inclined to form spherical clusters.

It has been well investigated that KBr (mainly the Br^-) is able to direct the growth of plate-like Au nanocrystals.[44−46] To investigate the role of KBr in our synthesis route, four solutions with different KBr concentrations are analyzed to prepare Au nanohydrangeas. Figure 5 shows the SEM images of the as-prepared Au nanohydrangeas with 0, 0.5, 1.25, and 5 mL of KBr (50 mM) in the reaction system. When free of KBr, it forms Au nanoparticle assemblies in a loosely bound manner (Figure 5a,e). When we use 0.5 mL of KBr as the surfactant, some of the plate-like petals have been observed, presenting a tendency to grow into nanohydrangeas, but there are still many nanoparticles attached to the petal surface (Figure 5b,f). When the surfactant concentration is increased to 1.25 mL, the morphology of Au nanohydrangeas becomes more distinguished (Figure 5c,g). As mentioned above, Br^- can facilitate the anisotropic growth of plate-like Au structures along the (111) plane and guide the growth of 2-D Au nanoplates and nanobelts. In our work, it reshapes the nanoparticles in a manner of promoting the growth of thin 2-D Au protrusions

https://doi.org/10.1021/acsomega.3c01802
ACS Omega 2023, 8, 26973−26981

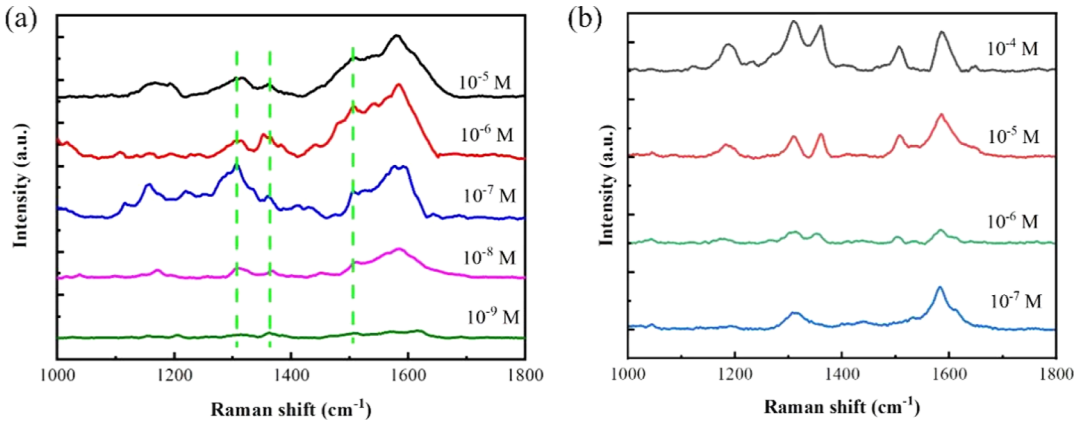

Figure 7. (a) SERS performance of the PDA/PVA/CNT foam−Au nanohydrangea substrate fabricated with 2.5 mL $HAuCl_4$ for detection of R6G from 10^{-5} to 10^{-9} M. (b) SERS performance of the PDA/PVA/CNT foam−Au nanoparticle substrate for detection of R6G from 10^{-4} to 10^{-7} M.

extending out of the main body of the particles. Eventually, they grow into a hydrangea-like structure. However, when the KBr concentration is as high as 5 mL, we notice the structure of the Au nanohydrangeas becomes irregular, and more plate-like petals extend out (Figure 5d,h). Over-load Br^- could restrain the growth of well-shaped Au nanocrystals, which is also reported previously.[12] To conclude, a moderate amount of KBr is essential to obtain regular Au nanohydrangeas. Therefore, it is important to control the concentration of KBr to have high-yield Au nanohydrangeas.

Accordingly, we summarize the growth process of the Au nanohydrangeas on PDA/PVA/CNT foams, as schematically demonstrated in Figure 6. In the first stage, with the aid of PDA reduction, the Au ions are formed into atoms, which spontaneously nucleate into nuclei, followed by the formation of clusters. Subsequently, these Au clusters start to grow into nanoparticles of different sizes. Small nanoparticles dissolve preferentially and precipitate on the surface of the larger nanoparticles, while the large nanoparticles continue to grow bigger at the cost of small nanoparticle consumption; i.e., they enter the ripening stage, and the basic outline of hydrangeas forms at this stage. Researchers have reported that halide ions such as bromide ions playing the role of capping agents can preferentially adsorb to specific gold nuclei facets, promoting the growth of plat-like Au structures along the (111) plane and guiding the growth of 2-D Au nanoplates and nanobelts;[13,44,45] which is consistent with our research. In our work, free Br^- ions are preferentially adsorbed to certain facets of the Au nanocrystal, guiding the growth of the Au nanocrystal along the (111) facets so that many plate-like petals grow out of the hydrangea base. Finally, more and more Au atoms are deposited along the (111) facets over time, thus forming an Au nanohydrangea structure with many plates cross-aligned. This also correlates with the XRD result that the intensity ratio of Au(111) to Au(200) is higher than that of randomly distributed polycrystalline Au nanocrystals/nanoparticles. However, due to technical difficulties in the direct observations of the growth process, the explicit mechanism of Br^- directing the growth of Au nanohydrangeas needs an in-depth further study in the future.

The sensitivity of SERS sensors strongly depends on the intensity of hot spots decorated on the SERS substrates. Anisotropic shapes of plasmonic nanostructures, such as sharp corners, protruded facets, and spurs extending out from nanoparticles, usually act as hot spots to provide the enhancement of Raman scattering.[47,48] To investigate the sensitivity of the CNT foam−Au nanohydrangeas SRES substrate, we use R6G as the analyte. Figure 7a shows the SERS spectra of R6G with a range from 10^{-5} to 10^{-9} M on the fabricated SERS substrate. It is well known that the characteristic Raman peaks of solid R6G are located at 1182, 1306, 1362, 1506, and 1647 cm^{-1} on the Raman spectrum.[12] There are many small peaks in the Raman spectra, and the characteristic peak of R6G located at 1182 cm^{-1} is not clearly captured, which is attributed to the PDA coating (we find that the N element from PDA covers some part of the hydrangeas, as shown from the EDS mapping). It can be clearly observed from the TEM image that the Au nanohydrangeas are tightly wrapped by the PDA, and the thickness of the PDA coating is not uniform, with a thickness of some parts up to 28.6 nm (Figure S6). Such a high thickness of the PDA coating hinders its detection sensitivity as a SERS substrate. As previously reported, the enhancement effect of the SERS substrate decreases with increasing polymer shell thickness.[49,50] Ye et al. found that the characteristic peak of 4-mercaptobenzoic acid with a concentration of 10^{-4} M becomes very weak when the PDA coating thickness of Au nanoparticles reaches 8.6 nm.[50] However, the synthesis of Au nanohydrangeas requires a sufficient amount of PDA on the CNT foams, which is difficult to avoid the encapsulation of PDA on the hydrangeas' surface. On the other hand, the Raman spectrum of the PDA/PVA/CNT foam−Au nanohydrangeas hybrid also confirms that the thickness of the PDA coating is too thick, which can seriously hinder its detection of R6G (Figure S7). Accordingly, we carried out a series of trials to remove the PDA, including washing, heat treatment, and chemical degradation; however, the results were not as effective as we expected (data not shown here). We have to note that the removal of PDA to improve the SERS's performance will be our focus in future work. Due to the high intensity of the G (1580 cm^{-1}) peak of CNT, the characteristic peak of R6G at 1647 cm^{-1} is not well distinguished, either. However, fingerprint peaks of R6G at 1306, 1362, and 1506 cm^{-1} can be undoubtedly seen in the Raman spectrum, which clearly confirms the detection of the analyte when its concentration falls in the range of 10^{-5} to 10^{-8} M. It is not difficult to find that the intensity of the characteristic Raman peaks of R6G becomes weaker as its concentration decreases. Although the intensity of the characteristic peaks is relatively weak when the concentration of R6G is reduced to 10^{-9} M, the three fingerprint peaks can

https://doi.org/10.1021/acsomega.3c01802
ACS Omega 2023, 8, 26973−26981

still be well resolved. However, when the concentration is reduced to 10^{-10} M, it can hardly obtain the Raman signal of R6G (data not shown here), indicating the detecting limitation of our SERS substrate is 10^{-9} M. In addition to the limit of detection, the enhancement factor (EF) is also an important parameter to evaluate the performance of SERS substrates, and we calculate the EF of PDA/PVA/CNT foam−Au nanohydrangeas substrate using the following equation

$$\mathrm{EF} = (I_{\mathrm{SERS}} \times N_{\mathrm{Raman}})/(I_{\mathrm{Raman}} \times N_{\mathrm{SERS}})$$

where I_{SERS} and I_{Raman} are the Raman intensities of analytes adsorbed on the SERS and normal substrates under the same conditions, respectively. N_{Raman} represents the number of molecules in the effective region on the normal substrate, and N_{SERS} represents the number of molecules in the effective region on the SERS substrate.[46] We chose the intensity of the Raman peak at 1360 cm^{-1} to evaluate the EF. The EF is calculated to be 7.6×10^7 when 10^{-9} M R6G is adsorbed on PDA/PVA/CNT foam−Au substrate. The high EF of PDA/PVA/CNT foam−Au nanospheres can be attributed to the high-density "hot spots". The unique three-dimensional structure of Au nanohydrangeas, combined with the large volume−surface area ratio, results in the three-dimensional spatial distribution of plasma hotspots as well as multiple plasmon resonance modes on PDA/PVA/CNT foam−Au nanohydrangea substrates. First, a strong local electromagnetic field can be generated from the gap between closely adjacent gold nanohydrangeas, which leads to the excitation of the gap plasma pattern.[51−53] Second, for a single Au nanohydrangea, the tips of its sharp petals can produce tip-like local electromagnetic field enhancement.[54] However, the higher density of hotspots is mainly attributed to its rich petal gaps and large rough petal surfaces. In addition, for a single Au nanohydrangea, the enhancement of an electromagnetic field can also be generated between the overlapping petals of its adjacent upper and lower layers.[54] The localized plasmon resonances in these different regions can be coupled to enhance the local electric field, resulting in a much stronger Raman signal. To better demonstrate the structural advantages of Au nanohydrangeas in SERS sensor applications, we employ the hybrid of PDA/PVA/CNT foam−Au nanoparticles as the SERS substrate to pursue the detection limit. Figure 7b shows the SERS spectra of R6G with a range from 10^{-4} to 10^{-7} M on a PDA/PVA/CNT foam−Au nanoparticle substrate. Interestingly, four Raman peaks (1182, 1306, 1362, and 1506 cm^{-1}) instead of three of R6G are captured, which is likely due to the high loading density of Au nanoparticles on the CNT support and the partial coverage of PDA on these plasmonic nanoparticles. However, the detection limit of R6G using the Au nanoparticle substrate is only 10^{-7} M, which is 2 orders of magnitude higher than that of the Au nanohydrangea substrate, further demonstrating the structural advantage of Au nanohydrangeas with respect to the application as SERS substrates.

Furthermore, we compared the recent reports on SERS sensors made of carbon nanomaterial-supported Au nanostructures. It has been reported that SERS substrates decorated with regular-shaped nanostructures containing tips and sharp edges (nanobelts, nanoframes, etc.) are more effective than those with spherical nanoparticles due to the high charging intensity at tips and edges.[48] The results of this work also prove this point. However, the detection limit of CNT foam−Au nanohydrangeas in this work is comparable to that of carbon nanomaterial-supported other shapes such as Au nanoframes and nanorods,[46,55] although Au hydrangeas as 3-D nanostructures present more tips, sharp edges, and large rough surface areas than Au nanoframes. Because the carbon nanomaterials they used, such as graphene and graphene oxide platforms, which has additive effects on the SERS sensitivity,[46] which, to some extent, may compensate for the weakness of nanostructures. On the other hand, the Au nanohydrangeas capped with PDA also hinder SERS performance. Similarly, the GO−Au nanostar hybrid SERS substrate combines the structural advantages of Au nanostars with the excellent adsorption properties of GO to exhibit optimal SERS performance. Therefore, in addition to the structure of Au nanocrystals, the neatness of their surface and the choice of substrate materials will affect SERS performance as well.

CONCLUSIONS

In summary, we devise a novel strategy to grow high-yield Au nanohydrangeas on 3-D CNT foams and use the hybrid as a SERS substrate. In the strategy, the surface of the as-prepared CNT foam is modified with PVA and PDA to get certain mechanical properties as well as surface activity. In the preparation of Au nanohydrangeas, the CNT foam with large pores and inter-space provides the growth room for high-yield Au nanocrystals. Meanwhile, PDA adsorbed on CNT surfaces is used as an efficient reducing agent as well as the provider of anchoring sites for Au nanohydrangeas. Moreover, the concentrations of synthetic reagents (e.g., $HAuCl_4$ and KBr) have a strong influence on the structure of Au nanohydrangeas, which means the appropriate amount, i.e., not too low nor too high, of these reagents is required to obtain the high-yield Au nanohydrangeas. The growth mechanism is discussed, which is supposed to be the directing function of Br^- ions. Benefiting from the regular and dense protruded facets of nanohydrangeas, the SERS substrates made of CNT foam and Au nanohydrangeas show a detection limit down to 10^{-9} M. This work confirms that high-yield Au nanohydrangeas can be deposited on CNT substrates by a simple wet-chemistry route and CNT-supported Au nanohydrangeas can be employed as SERS sensors. We hope that this work can shed some light on the controllable growth of noble metal nanocrystals as well as on the design of high-performance sensors based on these nanomaterials.

ASSOCIATED CONTENT

Supporting Information

The Supporting Information is available free of charge at https://pubs.acs.org/doi/10.1021/acsomega.3c01802.

SEM images of the raw CNT sheet, cross sections of the PDA/PVA/CNT foam, and PDA/PVA/CNT foam−Au nanohydrangeas; samples synthesized on PDA/PVA/CNT foams decorated with different amounts of DA; Au nanohydrangeas synthesized with 5 mL of $HAuCl_4$; TEM image of the Au nanohydrangea petal; and Raman spectrum of PDA/PVA/CNT−Au nanohydrangeas (PDF)

AUTHOR INFORMATION

Corresponding Author

Wenbo Xin − *College of Materials Science and Engineering, Nanjing Tech University, Nanjing, Jiangsu 211816, China;* orcid.org/0000-0001-6984-4242; Email: xinwenbo@njtech.edu.cn

https://doi.org/10.1021/acsomega.3c01802
ACS Omega 2023, 8, 26973−26981

Authors

Rong Yang − *College of Materials Science and Engineering, Nanjing Tech University, Nanjing, Jiangsu 211816, China*

Zhen Zhang − *Shandong Institute of Hydrogen Energy Technology, Jinan, Shandong 250000, China; China EV100 Hydrogen Center, Intelligent Manufacturing Workshop, Beijing 100096, China*

Naiqian Miao − *Shandong Institute of Hydrogen Energy Technology, Jinan, Shandong 250000, China; China EV100 Hydrogen Center, Intelligent Manufacturing Workshop, Beijing 100096, China*

Weichen Fang − *College of Materials Science and Engineering, Nanjing Tech University, Nanjing, Jiangsu 211816, China*

Zuo Xiao − *College of Materials Science and Engineering, Nanjing Tech University, Nanjing, Jiangsu 211816, China*

Xiaodong Shen − *College of Materials Science and Engineering, Nanjing Tech University, Nanjing, Jiangsu 211816, China;* orcid.org/0000-0002-6741-0667

Complete contact information is available at: https://pubs.acs.org/10.1021/acsomega.3c01802

Notes

The authors declare no competing financial interest.

■ ACKNOWLEDGMENTS

We acknowledge the start-up funding support from Nanjing Tech University. We also gratefully thank the support from the Shandong Institute of Hydrogen Energy Technology.

■ REFERENCES

(1) Lim, D. K.; Jeon, K. S.; Kim, H. M.; Nam, J. M.; Suh, Y. D. Nanogap-engineerable Raman-active nanodumbbells for single-molecule detection. *Nat. Mater.* **2010**, *9*, 60−67.

(2) Lin, M. H.; Sun, L.; Kong, F. B.; Lin, M. S. Rapid detection of paraquat residues in green tea using surface-enhanced Raman spectroscopy (SERS) coupled with gold nanostars. *Food Control* **2021**, *130*, 108280.

(3) Itoh, T.; Prochazka, M.; Dong, Z. C.; Ji, W.; Yamamoto, Y. S.; Zhang, Y.; Ozaki, Y. Toward a New Era of SERS and TERS at the Nanometer Scale: From Fundamentals to Innovative Applications. *Chem. Rev.* **2023**, *123*, 1552−1634.

(4) Tang, S. Y.; Li, Y.; Huang, H.; Li, P. H.; Guo, Z. N.; Luo, Q.; Wang, Z.; Chu, P. K.; Li, J.; Yu, X. F. Efficient Enrichment and Self-Assembly of Hybrid Nanoparticles into Removable and Magnetic SERS Substrates for Sensitive Detection of Environmental Pollutants. *ACS Appl. Mater. Interfaces* **2017**, *9*, 7472−7480.

(5) Shanta, P. V.; Cheng, Q. Graphene Oxide Nanoprisms for Sensitive Detection of Environmentally Important Aromatic Compounds with SERS. *ACS Sens.* **2017**, *2*, 817−827.

(6) Song, C. Y.; Yang, B. Y.; Zhu, Y.; Yang, Y. J.; Wang, L. H. Ultrasensitive sliver nanorods array SERS sensor for mercury ions. *Biosens. Bioelectron.* **2017**, *87*, 59−65.

(7) Yilmaz, M.; Babur, E.; Ozdemir, M.; Gieseking, R. L.; Dede, Y.; Tamer, U.; Schatz, G. C.; Facchetti, A.; Usta, H.; Demirel, G. Nanostructured organic semiconductor films for molecular detection with surface-enhanced Raman spectroscopy. *Nat. Mater.* **2017**, *16*, 918−924.

(8) Ben-Jaber, S.; Peveler, W. J.; Quesada-Cabrera, R.; Sol, C. W. O.; Papakonstantinou, I.; Parkin, I. P. Sensitive and specific detection of explosives in solution and vapour by surface-enhanced Raman spectroscopy on silver nanocubes. *Nanoscale* **2017**, *9*, 16459−16466.

(9) Sharma, B.; Frontiera, R. R.; Henry, A. I.; Ringe, E.; Van Duyne, R. P. SERS: Materials, applications, and the future. *Mater. Today* **2012**, *15*, 16−25.

(10) Orendorff, C. J.; Gole, A.; Sau, T. K.; Murphy, C. J. Surface-enhanced Raman spectroscopy of self-assembled monolayers: Sandwich architecture and nanoparticle shape dependence. *Anal. Chem.* **2005**, *77*, 3261−3266.

(11) Goul, R.; Das, S.; Liu, Q. F.; Xin, M.; Lu, R. T.; Hui, R.; Wu, J. Z. Quantitative analysis of surface enhanced Raman spectroscopy of Rhodamine 6G using a composite graphene and plasmonic Au nanoparticle substrate. *Carbon* **2017**, *111*, 386−392.

(12) Xin, W.; Yang, J. M.; Li, C.; Goorsky, M. S.; Carlson, L.; De Rosa, I. M. Novel Strategy for One-Pot Synthesis of Gold Nanoplates on Carbon Nanotube Sheet As an Effective Flexible SERS Substrate. *ACS Appl. Mater. Interfaces* **2017**, *9*, 6246−6254.

(13) Xin, W. B.; De Rosa, I. M.; Ye, P.; Severino, J.; Li, C.; Yin, X.; Goorsky, M. S.; Carlson, L.; Yang, J. M.; Yang, J. M. Graphene template-induced growth of single-crystalline gold nanobelts with high structural tunability. *Nanoscale* **2018**, *10*, 2764−2773.

(14) Xu, Y.; Wang, X. C.; Chen, L.; Zhao, Y.; He, L.; Yang, P. P.; Wu, H. H.; Bao, F.; Zhang, Q. High-yield synthesis of gold nanoribbons by using binary surfactants. *J. Mater. Chem. C* **2015**, *3*, 1447−1451.

(15) Duy, P. K.; Yen, P. T. H.; Chun, S.; Ha, V. T. T.; Chung, H. Carbon fiber cloth-supported Au nanodendrites as a rugged surface-enhanced Raman scattering substrate and electrochemical sensing platform. *Sens. Actuators, B* **2016**, *225*, 377−383.

(16) Demille, T. B.; Hughes, R. A.; Dominique, N.; Olson, J. E.; Rouvimov, S.; Camden, J. P.; Neretina, S. Large-area periodic arrays of gold nanostars derived from HEPES-DMF-and ascorbic-acid-driven syntheses. *Nanoscale* **2020**, *12*, 16489−16500.

(17) Xianyu, Y. L.; Lin, Y. Y.; Chen, Q.; Belessiotis-Richards, A.; Stevens, M. M.; Thomas, M. R. Iodide-Mediated Rapid and Sensitive Surface Etching of Gold Nanostars for Biosensing. *Angew. Chem., Int. Ed.* **2021**, *60*, 9891−9896.

(18) Kedia, A.; Kumar, P. S. Controlled reshaping and plasmon tuning mechanism of gold nanostars. *J. Mater. Chem. C* **2013**, *1*, 4540−4549.

(19) Riswana Barveen, N.; Wang, T. J.; Chang, Y. H. Photochemical synthesis of Au nanostars on PMMA films by ethanol action as flexible SERS substrates for in-situ detection of antibiotics on curved surfaces. *Chem. Eng. J.* **2022**, *431*, 134240.

(20) Wang, S. Q.; Xu, L. P.; Wen, Y. Q.; Du, H. W.; Wang, S. T.; Zhang, X. J. Space-confined fabrication of silver nanodendrites and their enhanced SERS activity. *Nanoscale* **2013**, *5*, 4284−4290.

(21) Huan, T. N.; Ganesh, T.; Kim, K. S.; Kim, S.; Han, S. H.; Chung, H. A three-dimensional gold nanodendrite network porous structure and its application for an electrochemical sensing. *Biosens. Bioelectron.* **2011**, *27*, 183−186.

(22) Chang, Y. H.; Liu, C.; Rouvimov, S.; Luo, T. F.; Feng, S. P. Electrochemical synthesis to convert a Ag film into Ag nanoflowers with high electrocatalytic activity. *Chem. Commun.* **2017**, *53*, 6752−6755.

(23) Ma, H. C.; Liu, Z. B.; Wei, Y. H.; Jiang, L. Controlled morphology evolution of branched Au nanostructures and their shape-dependent catalytic and photo-thermal properties. *Colloids Surf., A* **2019**, *582*, 123889.

(24) Jun, B. H.; Murata, M.; Hahm, E.; Lee, L. P. Synthesis method of asymmetric gold particles. *Sci. Rep.* **2017**, *7*, 2921.

(25) Song, C. Y.; Zhou, N.; Yang, B. Y.; Yang, Y. J.; Wang, L. H. Facile synthesis of hydrangea flower-like hierarchical gold nanostructures with tunable surface topographies for single-particle surface-enhanced Raman scattering. *Nanoscale* **2015**, *7*, 17004−17011.

(26) Wang, Z. Z.; Feng, Z. H.; Lin, L.; Huang, P. P.; Zheng, Z. Q. Top-down patterning and self-assembly of flower-like gold arrays for surface enhanced Raman spectroscopy. *Appl. Surf. Sci.* **2015**, *356*, 1314−1319.

(27) Zhao, Y. X.; Kang, H. S.; Zhao, W. Q.; Chen, Y. L.; Ma, L.; Ding, S. J.; Chen, X. B.; Wang, Q. Q. Dual Plasmon Resonances and Tunable Electric Field in Structure-Adjustable Au Nanoflowers for Improved SERS and Photocatalysis. *Nanomaterials* **2021**, *11*, 2176.

(28) Guo, S.; Wang, L.; Wang, E. Templateless, surfactantless, simple electrochemical route to rapid synthesis of diameter-controlled

3D flowerlike gold microstructure with "clean" surface. *Chem. Commun.* **2007**, 3163−3165.
(29) Wu, D.; Hu, M. N.; Zhang, Y. Y.; Zhou, J.; Wang, Z. N. Long-range ordered silver nanoflower array structure for surface enhanced Raman scattering detecting. *Appl. Surf. Sci.* **2020**, *505*, 144520.
(30) Pradhan, M.; Chowdhury, J.; Sarkar, S.; Sinha, A. K.; Pal, T. Hierarchical Gold Flower with Sharp Tips from Controlled Galvanic Replacement Reaction for High Surface Enhanced Raman Scattering Activity. *J. Phys. Chem. C* **2012**, *116*, 24301−24313.
(31) Lu, S. C.; You, T. T.; Gao, Y. K.; Yang, N.; Zhang, C. M.; Yin, P. G. Rapid fabrication of three-dimensional flower-like gold microstructures on flexible substrate for SERS applications. *Spectrochim. Acta, Part A* **2019**, *212*, 371−379.
(32) Hu, K.; Szkopek, T.; Cerruti, M. Tuning the aggregation of graphene oxide dispersions to synthesize elastic, low density graphene aerogels. *J. Mater. Chem. A* **2017**, *5*, 23123−23130.
(33) Liu, T.; Huang, M. L.; Li, X. F.; Wang, C. J.; Gui, C. X.; Yu, Z. Z. Highly compressible anisotropic graphene aerogels fabricated by directional freezing for efficient absorption of organic liquids. *Carbon* **2016**, *100*, 456−464.
(34) Mu, P.; Zhang, Z.; Bai, W.; He, J. X.; Sun, H. X.; Zhu, Z. Q.; Liang, W. D.; Li, A. Superwetting Monolithic Hollow-Carbon-Nanotubes Aerogels with Hierarchically Nanoporous Structure for Efficient Solar Steam Generation. *Adv. Energy Mater.* **2019**, *9*, 1802158.
(35) Wang, Z.; Zou, Y.; Li, Y. W.; Cheng, Y. Y. Metal-Containing Polydopamine Nanomaterials: Catalysis, Energy, and Theranostics. *Small* **2020**, *16*, 1907042.
(36) Kim, K. R.; Kim, J.; Kim, J. W.; Yavuz, C. T.; Yang, M. Y.; Nam, Y. S. Light-activated polydopamine coatings for efficient metal recovery from electronic waste. *Sep. Purif. Technol.* **2021**, *254*, 117674.
(37) Liu, B.; Wang, X. M.; Zhao, Y. W.; Wang, J. C.; Yang, X. L. Polymer shell as a protective layer for the sandwiched gold nanoparticles and their recyclable catalytic property. *J. Colloid Interface Sci.* **2013**, *395*, 91−98.
(38) Moraes, D. A.; Souza Junior, J. B.; Ferreira, F. F.; Mogili, N. V. V.; Varanda, L. C. Gold nanowire growth through stacking fault mechanism by oleylamine-mediated synthesis. *Nanoscale* **2020**, *12*, 13316−13329.
(39) Jatoi, A. W.; Ogasawara, H.; Kim, I. S.; Ni, Q. Q. Cellulose acetate/multi-wall carbon nanotube/Ag nanofiber composite for antibacterial applications. *Mater. Sci. Eng., C* **2020**, *110*, 110679.
(40) Li, Y. J.; Yang, M.; Xu, B. B.; Sun, Q. L.; Zhang, W.; Zhang, Y. J.; Meng, F. B. Synthesis, structure and antioxidant performance of boron nitride (hexagonal) layers coating on carbon nanotubes (multi-walled). *Appl. Surf. Sci.* **2018**, *450*, 284−291.
(41) Guo, Z. R.; Zhang, Y.; DuanMu, Y.; Xu, L.; Xie, S. L.; Gu, N. Facile synthesis of micrometer-sized gold nanoplates through an aniline-assisted route in ethylene glycol solution. *Colloids Surf., A* **2006**, *278*, 33−38.
(42) Son, H. Y.; Ryu, J. H.; Lee, H.; Nam, Y. S. Silver-Polydopamine Hybrid Coatings of Electrospun Poly(vinyl alcohol) Nanofibers. *Macromol. Mater. Eng.* **2013**, *298*, 547−554.
(43) Liang, M.; Zhang, G.; Feng, Y. J.; Li, R. L.; Hou, P.; Zhang, J. S.; Wang, J. M. Facile synthesis of silver nanoparticles on amino-modified cellulose paper and their catalytic properties. *J. Mater. Sci.* **2018**, *53*, 1568−1579.
(44) Kirner, F.; Potapov, P.; Schultz, J.; Geppert, J.; Muller, M.; Gonzalez-Rubio, G.; Sturm, S.; Lubk, A.; Sturm, E. Additive-controlled synthesis of monodisperse single crystalline gold nanoparticles: interplay of shape and surface plasmon resonance. *J. Mater. Chem. C* **2020**, *8*, 10844−10851.
(45) Soejima, T.; Kimizuka, N. One-Pot Room-Temperature Synthesis of Single-Crystalline Gold Nanocorolla in Water. *J. Am. Chem. Soc.* **2009**, *131*, 14407−14412.
(46) Ye, P. Y.; Xin, W. B.; De Rosa, I. M.; Wang, Y. K.; Goorsky, M. S.; Zheng, L.; Yin, X. Q.; Xie, Y. H. One-Pot Self-Templated Growth of Gold Nanoframes for Enhanced Surface-Enhanced Raman Scattering Performance. *ACS Appl. Mater. Interfaces* **2020**, *12*, 22050−22057.
(47) Orendorff, C. J.; Gole, A. M.; Sau, T. K.; Murphy, C. J. Surface-Enhanced Raman Spectroscopy of Self-Assembled Monolayers: Sandwich Architecture and Nanoparticle Shape Dependence. *Anal. Chem.* **2005**, *77*, 3261−3266.
(48) Kodiyath, R.; Malak, S. T.; Combs, Z. A.; Koenig, T.; Mahmoud, M. A.; El-Sayed, M. A.; Tsukruk, V. V. Assemblies of silver nanocubes for highly sensitive SERS chemical vapor detection. *J. Mater. Chem. A* **2013**, *1*, 2777−2788.
(49) Tegegne, W. A.; Mekonnen, M. L.; Beyene, A. B.; Su, W. N.; Hwang, B. J. Sensitive and reliable detection of deoxynivalenol mycotoxin in pig feed by surface enhanced Raman spectroscopy on silver nanocubes@polydopamine substrate. *Spectrochim. Acta, Part A* **2020**, *229*, 117940.
(50) Ye, W. C.; Huang, H.; Yang, W. W.; Wang, X.; Ren, C. L.; Hu, Q. S.; Li, Y. M.; Ren, B. Ultrathin polydopamine film coated gold nanoparticles: a sensitive, uniform, and stable SHINERS substrate for detection of benzotriazole. *Analyst* **2017**, *142*, 3459−3467.
(51) Kasera, S.; Biedermann, F.; Baumberg, J. J.; Scherman, O. A.; Mahajan, S. Quantitative SERS Using the Sequestration of Small Molecules Inside Precise Plasmonic Nanoconstructs. *Nano Lett.* **2012**, *12*, 5924−5928.
(52) Yu, M. D.; Huang, Z. P.; Liu, Z. Q.; Chen, J.; Liu, Y.; Tang, L.; Liu, G. Q. Annealed gold nanoshells with highly-dense hotspots for large-area efficient Raman scattering substrates. *Sens. Actuators, B* **2018**, *262*, 845−851.
(53) Tian, H. H.; Li, H. B.; Fang, Y. Binary Thiol-Capped Gold Nanoparticle Monolayer Films for Quantitative Surface-Enhanced Raman Scattering Analysis. *ACS Appl. Mater. Interfaces* **2019**, *11*, 16207−16213.
(54) Liu, G. Q.; Liu, Y.; Tang, L.; Liu, X. S.; Fu, G. L.; Liu, Z. Q. Semiconductor-enhanced Raman scattering sensors via quasi-three-dimensional Au/Si/Au structures. *Nanophotonics* **2019**, *8*, 1095−1107.
(55) Chong, H. B.; Gao, G. Q.; Li, G. Recyclable substrates based on graphene oxide/gold nanorod composites for efficient surface enhanced Raman scattering. *New J. Chem.* **2020**, *44*, 704−708.

https://doi.org/10.1021/acsomega.3c01802
ACS Omega 2023, 8, 26973−26981